JCTC Journal of Chemical Theory and Computation

Article

Cite This: J. Chem. Theory Comput. 2019, 15, 6703−6711

pubs.acs.org/JCTC

Stochastic Resolution of Identity for Real-Time Second-Order Green's Function: Ionization Potential and Quasi-Particle Spectrum

Wenjie Dou,*,† Tyler Y. Takeshita,*,‡ Ming Chen,*,†,§ Roi Baer,*,∥ Daniel Neuhauser,*,⊥ and Eran Rabani*,†,§,#

†Department of Chemistry, University of California Berkeley, Berkeley, California 94720, United States

‡Mercedes-Benz Research and Development North America, Sunnyvale, California 94085, United States

§Materials Sciences Devision, Lawrence Berkeley National Laboratory, Berkeley, California 94720, United States

∥Fritz Haber Research Center for Molecular Dynamics, Institute of Chemistry, The Hebrew University of Jerusalem, Jerusalem 9190401, Israel

⊥Department of Chemistry and Biochemistry, University of California Los Angeles, Los Angeles, California 90095, United States

#The Raymond and Beverly Sackler Center of Computational Molecular and Materials Science, Tel Aviv University, Tel Aviv 69978, Israel

ABSTRACT: We develop a stochastic resolution of identity approach to the real-time second-order Green's function (real-time sRI-GF2) theory, extending our recent work for imaginary-time Matsubara Green's function [Takeshita et al. *J. Chem. Phys.* **2019**, *151*, 044114]. The approach provides a framework to obtain the quasi-particle spectra across a wide range of frequencies and predicts ionization potentials and electron affinities. To assess the accuracy of the real-time sRI-GF2, we study a series of molecules and compare our results to experiments as well as to a many-body perturbation approach based on the GW approximation, where we find that the real-time sRI-GF2 is as accurate as self-consistent GW. The stochastic formulation reduces the formal computatinal scaling from $O(N_e^5)$ down to $O(N_e^3)$ where N_e is the number of electrons. This is illustrated for a chain of hydrogen dimers, where we observe a slightly lower than cubic scaling for systems containing up to $N_e \approx 1000$ electrons.

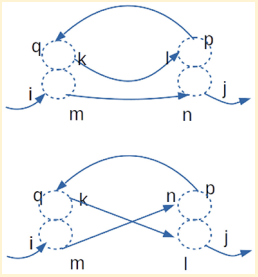

1. INTRODUCTION

Recently there has been an increased interest in electronic structure methods capable of accurately describing quasi-particle spectra and in particular the ionization potential (IP) and electron affinity (EA). Density functional theory (DFT) has been the most commonly used tool for predicting ground state properties for molecular and extended systems.[1−4] Besides these properties, Kohn−Sham (KS)[5,6] DFT offers a framework for calculating the IPs from the orbital energy of the highest occupied molecular orbital (HOMO), provided that exact exchange−correlation functionals are given.[7,8] However, in practice, the exact exchange−correlation functionals are not known, and the IPs from KS-DFT are often off by several electronvolts in comparison to experiments.[9]

The accurate description of quasi-particles has greatly benefited from Green's function techniques, mainly within the many-body perturbation theory (MBPT). These methods have proven extremely fruitful and allow the inclusion of electron correlation through systematic approximations of the self-energy, enabling an accurate description of quasi-particle energies and lifetimes. The most common flavor of Green's function methods used is the GW approximation,[10] where G indicates the single-particle Green function and W is the screened Coulomb interaction. This method offers improved accuracy over DFT in describing quasi-particle properties including IPs and EAs in bulk systems.[11−27] In the GW approximation the contribution of exact exchange, while very large, is only applied statically. The only dynamic part in the approximation is based on random-phase approximation (RPA) without exchange. The validity of this limitation when applied to molecular systems remains an active area of research.[28,29]

An alternative to the GW approximation is the second-order self-energy approximation, or the Green's function 2 (GF2) method, where the self-energy is expanded to second order in the Coulomb interaction.[30−39] In contrast to GW, GF2 includes exchange effects explicitly, beyond the static level, in the self-energy but treats the polarization term differently than GW. A key limitation of the GF2 method is the $O(N_e^5)$ scaling of the second-order exchange term in the self-energy, restricting its applications to small molecular systems. Inspired by recent developments,[39] we have introduced a stochastic resolution of identity (sRI)[40] implementation of the Matsubara GF2 approach for the calculation of ground state properties within the second-order Green's function approach.[41] The sRI technique reduced the computational cost of the second-order self-energy method to $O(N_e^3)$, and was applied to systems with more than 1000 electrons.

Received: September 16, 2019
Published: October 25, 2019

DOI: 10.1021/acs.jctc.9b00918
J. Chem. Theory Comput. 2019, 15, 6703−6711

In the current work, we expand our approach and develop a stochastic version of *real-time* GF2 theory. This provides a framework to calculate quasi-particle properties, electron affinities, and ionization potentials with a reduced scaling of $O(N_e^3)$. To be clear, in this work, we do not consider a time-dependent perturbation potential and only propagate the single-particle Green's functions along one real-time axis; i.e., we are considering only an equilibrium scenario. The stochastic real-time GF2 approach developed here has similar flavor with previous stochastic versions of electronic structure theories, e.g., MP2,[40,42,43] RPA,[44] DFT,[45−48] and GW.[49] Among the methods listed, this work is closest to the stochastic implementation of Matsubara GF2 theory.[41] We illustrate the accuracy of the approach for a set of molecules and compare the IPs to experiments and GW results. We find that the stochastic real-time GF2 method provides accurate IPs that are in good agreement with experiments and with the self-consistent GW method.

The article is organized as follows: In section 2 we provide the basic theory for obtaining the quasi-particle spectrum from real-time propagation of the second-order Green's function. In section 3 we review our stochastic resolution of identity and apply such techniques to real-time GF2 theory. In section 4 we report ionization potentials, quasi-particle spectra, and timing from real-time GF2 theory. Finally, in section 5, we conclude.

2. THEORY

Consider a general Hamiltonian for a many-body electronic system in second quantization:

$$\hat{H} = \sum_{ij} h_{ij}\hat{a}_i^\dagger \hat{a}_j + \sum_{ijkl} v_{ijkl}\hat{a}_i^\dagger \hat{a}_k^\dagger \hat{a}_l \hat{a}_j \tag{1}$$

where $\hat{a}_i^\dagger$ ($\hat{a}_i$) is the creation (annihilation) operator for an electron in atomic orbital $|\chi_i\rangle$. The creation and annihilation operators obey the following commutation relation:

$$[\hat{a}_i, \hat{a}_j^\dagger] = (\boldsymbol{S}^{-1})_{ij} \tag{2}$$

Here $\mathbf{S}$ is the overlap matrix for different orbitals, namely, $S_{ij} = \langle\chi_i|\chi_j\rangle$. In eq 1, h_{ij} are matrix elements of the noninteracting electronic Hamiltonian and v_{ijkl} are the four-index electron repulsion integrals:

$$v_{ijkl} = (ij|kl) = \iint \mathrm{d}\mathbf{r}_1\, \mathrm{d}\mathbf{r}_2\, \frac{\chi_i(\mathbf{r}_1)\,\chi_j(\mathbf{r}_1)\,\chi_k(\mathbf{r}_2)\,\chi_l(\mathbf{r}_2)}{|\mathbf{r}_1 - \mathbf{r}_2|} \tag{3}$$

where $\chi_i(\mathbf{r})$ is the position representation of $|\chi_i\rangle$.

2.1. Kadanoff−Baym Equations. The quantity of interest in this work is the single-particle Green's function on the Keldysh contour, defined as (we set $\hbar = 1$ throughout)[32,50]

$$G_{ij}(\tilde{t}_1, \tilde{t}_2) = -\mathrm{i}\langle T_C \hat{a}_i(\tilde{t}_1)\, \hat{a}_j^\dagger(\tilde{t}_2)\rangle \tag{4}$$

We use $\tilde{t}$ to denote a time point on a Keldysh contour defined on the real axis from 0 to positive infinity $(0, +\infty)$, then back to the origin $(+\infty, 0)$, finally to $-\mathrm{i}\beta$ on the imaginary axis $(0, -\mathrm{i}\beta)$. T_C is a time ordering operator on the Keldysh contour. The operators in the above equations are defined in the Heisenberg representation such that $\hat{a}_i^\dagger(\tilde{t}_1) = \mathrm{e}^{\mathrm{i}\hat{H}\tilde{t}_1}\hat{a}_i^\dagger \mathrm{e}^{-\mathrm{i}\hat{H}\tilde{t}_1}$. The average in the above is taken with respect to a Boltzmann distribution: $\langle\cdots\rangle = Z^{-1}\,\mathrm{Tr}[(\cdots)\mathrm{e}^{-\beta(\hat{H}-\mu\hat{N})}]$, where $Z = \mathrm{Tr}[\mathrm{e}^{-\beta(\hat{H}-\mu\hat{N})}]$ is the grand-canonical partition function, $\beta = \frac{1}{k_B T}$ is the inverse temperature, and μ is the chemical potential. The number operator is given by $\hat{N} = \sum_{ij} S_{ij}\hat{a}_i^\dagger \hat{a}_j$.

The equation of motion for the Green's function defined in eq 4 satisfies the Kadanoff−Baym equation:

$$\mathrm{i}\mathbf{S}\partial_{\tilde{t}_1}\mathbf{G}(\tilde{t}_1, \tilde{t}_2) = \delta(\tilde{t}_1, \tilde{t}_2) + \mathbf{F}\mathbf{G}(\tilde{t}_1, \tilde{t}_2) + \int_C \mathbf{\Sigma}(\tilde{t}_1, \tilde{t}_3)\,\mathbf{G}(\tilde{t}_3, \tilde{t}_2)\,\mathrm{d}\tilde{t}_3 \tag{5}$$

where $\mathbf{F}$ is the Fock matrix obtained from the imaginary-time Matsubara Green's function (see below for more details) and the time integration in the above equation is carried out on the Keldysh contour (C). In the second-order Born approximation, the matrix elements of the self-energy $\mathbf{\Sigma}(\tilde{t}_1, \tilde{t}_2)$ take the following form:

$$\Sigma_{ij}(\tilde{t}_1, \tilde{t}_2) = \sum_{klmnpq} G_{kl}(\tilde{t}_1, \tilde{t}_2)\, G_{mn}(\tilde{t}_1, \tilde{t}_2)\, G_{pq}(\tilde{t}_2, \tilde{t}_1)\, v_{imqk}(2v_{lpnj} - v_{nplj}) \tag{6}$$

In contrast to the GW approximation, in the second-order Born approximation, the exchange correlations are taken into account explicitly beyond the static part (see Figure 1). The factor 2 in eq 6 accounts for spin degeneracy. Note that for simplicity we have restricted ourselves to the closed-shell case, but extensions to open-shell systems are straightforward.

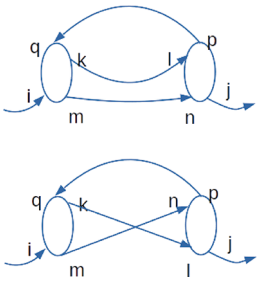

Figure 1. Second-order Born self-energy for molecules: direct (upper) and exchange (lower) correlations. See also eq 6. Note that the exchange correlations (lower) are not included in GW approximation.

To solve the Kadanoff−Baym equations requires a specific projection onto real and imaginary time branches of the Keldysh contour. In the present case (equilibrium), this requires only three types of GFs: When both times are projected onto the imaginary branch (Matsubara GF), when one time is projected onto the imaginary-time branch while the other is projected onto the real-time branch (mixed-time GF), and, finally, when both times are projected to the real-time branch for $t, t' > 0$ (retarded GF) in order to obtain the spectral function. In the following subsections we describe equations of motion for the three cases discussed above. We begin with the simplest case where both times are projected onto the imaginary axis.

2.2. Matsubara Green's Function. If we restrict $\tilde{t}_1$ and $\tilde{t}_2$ to the imaginary time branch ($\tilde{t}_1 = -\mathrm{i}\tau_1$, $\tilde{t}_2 = -\mathrm{i}\tau_2$), the Keldysh contour ordered Green's function in eq 4 reduces to the Matsubara Green's function, $\mathrm{i}\mathbf{G}^{\mathrm{M}}(\tau_1 - \tau_2) = \mathbf{G}(-\mathrm{i}\tau_1, -\mathrm{i}\tau_2)$, which only depends on the imaginary-time difference ($\tau = \tau_1 - \tau_2 \in [0, \beta]$). The superscript "M" stands for a Matsubara quantity. The equation of motion for the Matsubara Green's function can be written in an integral form:

DOI: 10.1021/acs.jctc.9b00918
J. Chem. Theory Comput. 2019, 15, 6703−6711

$$\mathbf{G}^{\mathrm{M}}(\tau) = \mathbf{G}_0^{\mathrm{M}}(\tau) + \int_0^\beta \mathrm{d}\tau'\, \mathrm{d}\tau''\, \mathbf{G}_0^{\mathrm{M}}(\tau - \tau')\, \mathbf{\Sigma}^{\mathrm{M}}(\tau' - \tau'')\, \mathbf{G}^{\mathrm{M}}(\tau'') \tag{7}$$

where $\mathbf{G}_0^{\mathrm{M}}(\tau)$ is the zero-order Matsubara Green's function given in terms of the Fockian:[41]

$$\mathbf{G}_0^{\mathrm{M}}(\tau) = \mathbf{X}\mathrm{e}^{-\tau(\bar{\mathbf{F}}-\mu\mathbf{I})}\left[\frac{\theta(-\tau)}{1+\mathrm{e}^{\beta(\bar{\mathbf{F}}-\mu\mathbf{I})}} - \frac{\theta(\tau)}{1+\mathrm{e}^{-\beta(\bar{\mathbf{F}}-\mu\mathbf{I})}}\right]\mathbf{X}^{\mathrm{T}} \tag{8}$$

In eq 8, $\mathbf{X}\mathbf{X}^{\mathrm{T}} = \mathbf{S}^{-1}$ and $\bar{\mathbf{F}} = \mathbf{X}^{\mathrm{T}}\mathbf{F}\mathbf{X}$. In the second-order Born approximation, the matrix elements of the Matsubara self-energy take the following form:

$$\Sigma_{ij}^{\mathrm{M}}(\tau) = \sum_{klmnpq} G_{kl}^{\mathrm{M}}(\tau)\, G_{mn}^{\mathrm{M}}(\tau)\, G_{pq}^{\mathrm{M}}(\beta - \tau)\, v_{imqk}(2v_{lpnj} - v_{nplj}) \tag{9}$$

Obviously, eqs 7–9 have to be solved self-consistently, since the self-energy itself depends on the Matsubara GF. Furthermore, for convenience we also update the Fock matrix according to[41] $F_{ij} = h_{ij} - 2\sum_{mn} G^{\mathrm{M}}(\tau{=}\beta)(v_{ijmn} - 1/2v_{inmj})$ and also adjust the chemical potential μ to conserve the number of electrons by imposing that $N_e = -2\sum_{mn} G^{\mathrm{M}}(\tau{=}\beta)S_{mn}$. In order to solve for the Matsubara Green's function in a numerically efficient way, proper quadratures and contractions are used to evaluate the double integral on the right-hand side of eq 7. See ref 41 for more details.

2.3. Equations of Motion for Mixed-Time Green's Function. In the absence of a time-dependent perturbation, it is sufficient to work with the mixed branch, such that the mixed-time Green's function is given by $\mathbf{G}^{\rceil}(t, \tau) = \mathbf{G}(\tilde{t}_1 = t, \tilde{t}_2 = -\mathrm{i}\tau)$. Using Langreth rules,[32] the equation of motion for the mixed-time Green's function can be written as

$$\mathrm{i}\mathbf{S}\partial_t\mathbf{G}^{\rceil}(t, \tau) = \mathbf{F}\mathbf{G}^{\rceil}(t, \tau) + \int_0^t \mathbf{\Sigma}^{\mathrm{R}}(t')\, \mathbf{G}^{\rceil}(t - t', \tau)\, \mathrm{d}t' + \int_0^\beta \mathbf{\Sigma}^{\rceil}(t, \tau_1)\, \mathbf{G}^{\mathrm{M}}(\tau_1 - \tau)\, \mathrm{d}\tau_1 \tag{10}$$

In eq 10, both $\mathbf{F}$ and $\mathbf{G}^{\mathrm{M}}(\tau_1 - \tau)$ are obtained from the solution of the Kadanoff–Baym equations in imaginary time as explained in section 2.2. In other words, the matrix elements of $\mathbf{F}$ are given by $F_{ij} = h_{ij} - 2\sum_{mn} G^{\mathrm{M}}(\tau{=}\beta)(v_{ijmn} - 1/2v_{inmj})$. The mixed-time self-energy within the second Born approximation is given by

$$\Sigma_{ij}^{\rceil}(t, \tau) = \sum_{klmnpq} G_{kl}^{\rceil}(t, \tau)\, G_{mn}^{\rceil}(t, \tau)\, G_{pq}^{\lceil}(t, \beta - \tau)^*\, v_{impk}(2v_{jnql} - v_{jlqn}) \tag{11}$$

where we have used the relation $G_{ji}^{\lceil}(\tau,t)^* = G_{ij}^{\rceil}(t, \beta - \tau)$ and defined $\mathbf{G}^{\lceil}(\tau,t) = \mathbf{G}(\tilde{t}_1 = -\mathrm{i}\tau, \tilde{t}_2 = t)$ to be consistent with the definition of $\mathbf{G}^{\rceil}(t,\tau)$. Finally, the retarded self-energy $\Sigma_{ij}^{\mathrm{R}}(t_1)$ is related to lesser and greater self-energies by the simple relation

$$\Sigma_{ij}^{\mathrm{R}}(t_1 - t_2) = \theta(t_1 - t_2)(\Sigma_{ij}^{>}(t_1 - t_2) - \Sigma_{ij}^{<}(t_1 - t_2)) \tag{12}$$

where $\theta(t)$ is the Heaviside step function and $\Sigma_{ij}^{<,>}(t)$ are the matrix elements of the lesser/greater self-energy. At equilibrium, the latter can be expressed in terms of the mixed-time self-energies:

$$\Sigma_{ij}^{<}(t) = \Sigma_{ij}^{\rceil}(t, \tau = 0) \tag{13}$$

$$\Sigma_{ij}^{>}(t) = -\Sigma_{ji}^{>}(-t)^* = -\Sigma_{ji}^{\lceil}(\tau = 0, t)^* = -\Sigma_{ij}^{\rceil}(t, \tau = \beta) \tag{14}$$

The equation of motion for $\mathbf{G}^{\rceil}(t,\tau)$ must be solved self-consistently, since the corresponding self-energies depend on the GF itself. The initial conditions for the mixed-time GF in eq 10 are given by $G_{ij}^{\rceil}(t = 0, \tau) = -\mathrm{i}G_{ij}^{\mathrm{M}}(\beta - \tau)$. In the numerical implementations, we have used the method of ref 51 to propagate the mixed-time GFs. Similar to the case of pure imaginary time, the last term in eq 10 is evaluated through proper quadrature.[41]

2.4. Observables and Quasi-Particle Spectrum. In order to calculate the spectral functions within the second-order Green's function approach, one requires the lesser and greater Green's functions. These can be obtained directly from $G^{\rceil}(t_1,\tau)$ as follows (relation holds for equilibrium only):

$$G_{ij}^{<}(t) = G_{ij}^{\rceil}(t, \tau = 0) \tag{15}$$

$$G_{ij}^{>}(t) = -G_{ji}^{>}(-t)^* = -G_{ji}^{\lceil}(\tau = 0, t)^* = -G_{ij}^{\rceil}(t, \tau = \beta) \tag{16}$$

Furthermore, the retarded Green's function can be expressed in terms of the lesser/greater GFs as follows:

$$G_{ij}^{\mathrm{R}}(t) = \theta(t)(G_{ij}^{>}(t) - G_{ij}^{<}(t)) \tag{17}$$

and spectral function $A(\omega)$ is then defined as the imaginary portion of the retarded Green's function:

$$A(\omega) = -\sum_{mn} \mathrm{Im}\, \tilde{G}_{mn}^{\mathrm{R}}(\omega) S_{mn} \tag{18}$$

where $\tilde{\mathbf{G}}^{\mathrm{R}}(\omega)$ is the Fourier transform of $\mathbf{G}^{\mathrm{R}}(t)$

$$\tilde{\mathbf{G}}^{\mathrm{R}}(\omega) = \int_{-\infty}^{\infty} \mathrm{d}t\, \mathbf{G}^{\mathrm{R}}(t)\mathrm{e}^{\mathrm{i}\omega t} \tag{19}$$

As can be clearly seen, the spectral function can be obtained directly from the mixed-time $G_{ij}^{\rceil}(t,\tau)$.

3. STOCHASTIC RESOLUTION OF IDENTITY

Similar to the Matsubara GF2 case, the computational bottleneck in real-time propagation of the Green's function is the evaluation of the self-energy in eq 11, which scales as $O(N_e^5)$. To overcome this steep computational scaling, we have developed a stochastic resolution of identity (sRI) for Matsubara GF2 theory, which reduces the computational cost of the self-energy to $O(N_e^3)$.[40,41] The same technique is applied here to the mixed-time formulation. In this section, we briefly review the sRI theory and show how sRI formulation can be used to reduce the computational cost in evaluation of the mixed-time self-energy.

Before introducing sRI, we first review the RI. The four-index electron repulsion integral (ERI) defined in eq 3 can be approximated by

$$(ij|mn) \approx \sum_{AB}^{N_{\mathrm{aux}}} (ij|A)V_{AB}^{-1}(B|mn) \tag{20}$$

where we have defined the three-index ERI and two-index ERI as follows:

DOI: 10.1021/acs.jctc.9b00918
J. Chem. Theory Comput. 2019, 15, 6703–6711

$$(ij|A) = \iint \mathrm{d}r_1\, \mathrm{d}r_2\, \frac{\chi_i(r_1)\,\chi_j(r_1)\,\chi_A(r_2)}{r_{12}} \tag{21}$$

$$V_{AB} = \iint \mathrm{d}r_1\, \mathrm{d}r_2\, \frac{\chi_A(r_1)\,\chi_B(r_2)}{r_{12}} \tag{22}$$

Here, χ_A and χ_B are auxiliary orbitals.

In a stochastic resolution of identity approach, an additional set of N_s *stochastic orbitals* are introduced, $\{\theta^\xi\}$, $\xi = 1, 2, ..., N_s$. Here θ^ξ is a vector of length N_{aux} (N_{aux} is the size of the auxiliary basis). The elements in θ^ξ are randomly chosen from a uniform distribution of ± 1, $\theta_A^\xi = \pm 1$ ($A = 1, 2, ..., N_{aux}$), and satisfy the relation

$$\lim_{N_s\to\infty} \frac{1}{N_s} \sum_{\xi}^{N_s} \theta_A^\xi \theta_B^\xi = \delta_{AB} \tag{23}$$

Using the stochastic orbitals, eq 20 can be expressed as follows:

$$\begin{aligned}
&\sum_{AB}^{N_{aux}} (ij|A) V_{AB}^{-1} (B|mn) \\
&= \sum_{PQ}^{N_{aux}} \sum_{AB}^{N_{aux}} (ij|A) V_{AP}^{-1/2} \delta_{PQ} V_{QB}^{-1/2} (B|mn) \\
&\to \frac{1}{N_s} \sum_{\xi}^{N_s} \sum_{PQ}^{N_{aux}} \sum_{AB}^{N_{aux}} (ij|A) V_{AP}^{-1/2} \theta_P^\xi \theta_Q^\xi V_{QB}^{-1/2} (B|mn) \\
&= \frac{1}{N_s} \sum_{\xi}^{N_s} \left[\sum_{A}^{N_{aux}} (ij|A) \sum_{P}^{N_{aux}} V_{AP}^{-1/2} \theta_P^\xi \right] \left[\sum_{B}^{N_{aux}} (B|mn) \sum_{Q}^{N_{aux}} \theta_Q^\xi V_{QB}^{-1/2} \right]
\end{aligned} \tag{24}$$

The four-index ERI (eq 20) now can be approximated by an average over number of stochastic orbitals:

$$(ij|mn) \approx \frac{1}{N_s} \sum_{\xi} R_{ij}^\xi R_{mn}^\xi \equiv \langle R_{ij} R_{mn} \rangle_\xi \tag{25}$$

where R_{ij}^ξ is given by

$$R_{ij}^\xi = \sum_{A}^{N_{aux}} (ij|A) \left[\sum_{P}^{N_{aux}} V_{AP}^{-1/2} \theta_P^\xi \right] \tag{26}$$

The advantages of introduction of sRI over RI have been discussed extensively in our previous work.[40,41] In particular, sRI reduces the overall computational scaling since the number of stochastic orbitals does not increase with system size. The current focus of this paper is to apply the sRI method to our real-time GF2 theory.

3.1. sRI Applied to Real-Time Second Born Approximation. In the current formulation, we apply the sRI to the second Born approximation for the real-time self-energy, which takes the form of eq 27.

$$\begin{aligned}
\Sigma_{ij}^{]}(t_1, \tau) &= \langle \sum_{klmnpq} G_{kl}^{]}(t_1, \tau) G_{mn}^{]}(t_1, \tau) G_{pq}^{]}(t_1, \beta - \tau)^* R_{ik} R_{mq} (2R'_{lj} R'_{pn} - R'_{nj} R'_{lp}) \rangle_{\zeta,\zeta'} \\
&= \langle \sum_{klmnpq} 2G_{kl}^{]}(t_1, \tau) G_{mn}^{]}(t_1, \tau) G_{pq}^{]}(t_1, \beta - \tau)^* R_{ik} R_{mq} R'_{lj} R'_{pn} - G_{kl}^{]}(t_1, \tau) G_{mn}^{]}(t_1, \tau) G_{pq}^{]}(t_1, \beta - \tau)^* R_{ik} R_{mq} R'_{nj} R'_{lp} \rangle_{\zeta,\zeta'} \\
&= \Sigma_{ij}^{\mathrm{dir},]}(t, \tau) + \Sigma_{ij}^{\mathrm{ex},]}(t, \tau)
\end{aligned} \tag{27}$$

In eq 27 $\mathbf{R}$ and $\mathbf{R}'$ are uncorrelated stochastic matrices generated using a different set of stochastic orbitals (eq 25) and the direct and exchange terms of the self-energies are given by eq 28.

$$\begin{aligned}
\Sigma_{ij}^{\mathrm{dir},]}(t, \tau) &= \langle \sum_{klmnpq} 2G_{kl}^{]}(t_1, \tau) G_{mn}^{]}(t_1, \tau) G_{pq}^{]}(t_1, \beta - \tau)^* R'_{lj} R'_{pn} \rangle_{\zeta,\zeta'} \\
\Sigma_{ij}^{\mathrm{ex},]}(t, \tau) &= \langle - \sum_{klmnpq} G_{kl}^{]}(t_1, \tau) G_{mn}^{]}(t_1, \tau) G_{pq}^{]}(t_1, \beta - \tau)^* R_{ik} R_{mq} R'_{nj} R'_{lp} \rangle_{\zeta,\zeta'}
\end{aligned} \tag{28}$$

The above expressions for the mixed-time self-energy can be evaluated at $O(N_e^3)$ computational scaling (rather than $O(N_e^5)$) as long as the number of stochastic orbitals does not increase with the system size. This can be done by using contractions. Note that the sRI is used only for the evaluation of the self-energy while the remaining portion of the calculations is performed deterministically.

3.2. Summary of the Proposed Algorithm. To summarize this part, the real-time sRI-GF2 requires the following steps:

1. Perform a sRI-GF2 for the Matsubara Green's function as described in section 2.2 and in more detail in ref 41 to generate $\mathbf{G}^{\mathrm{M}}(\tau)$.
2. Use $\mathbf{G}^{\mathrm{M}}(\tau)$ as the initial condition for the mixed-time Green's function and solve eq 10 and obtain the mixed-time self-energy using eq 11.
3. Solve eq 10 to generate the mixed-time self-energy and eqs 12−14 to generate the retarded self-energy, $\Sigma_{ij}^{\mathrm{R}}(t)$. This is done "on the fly".
4. Propagate eq 10 until the self-energies decay to a predefined tolerance or until the final observables converge with respect to the propagation time.
5. Fourier transform $\Sigma_{ij}^{\mathrm{R}}(t)$ to the frequency domain and solve the Dyson equation for

$$\tilde{\mathbf{G}}^{\mathrm{R}}(\omega) = \frac{1}{\omega \mathbf{S} - \mathbf{F} - \tilde{\mathbf{\Sigma}}^{\mathrm{R}}(\omega)}$$

Use eq 18 to generate the spectral function, $A(\omega)$. Here, $\tilde{\mathbf{\Sigma}}^{\mathrm{R}}(\omega)$ is the Fourier transform of $\mathbf{\Sigma}^{\mathrm{R}}(t)$.

4. RESULTS AND DISCUSSION

In this section, we analyze the performance of the real-time sRI-GF2 theory, especially its ability to predicting IPs and quasi-particle spectra for molecules and for extended systems. The time step used to integrate eq 10 is $0.05 E_h^{-1}$ (E_h is

DOI: 10.1021/acs.jctc.9b00918
J. Chem. Theory Comput. 2019, 15, 6703−6711

Hartree energy),[29] unless otherwise noted. We set $\beta = 50E_h^{-1}$ and use 256 Chebyshev points and Gauss−Legendre quadratures to integrate the imaginary term in eq 10. In addition, a small damping term $\eta = 0.01E_h$ is added to the real-time propagation of the Green's function. Finally, a complementary error function $\mathrm{erfc}(t/t_{ce})$ is multiplied to $\Sigma^R(t)$ in order to prevent the instability of Fourier transform.[42,52]

4.1. Ionization Potentials for Molecules. The IP can be extracted from the quasi-particle spectrum $A(\omega)$ as the position of the peak near the highest occupied molecular orbital (HOMO). In this subsection, we compare IPs generated from the real-time sRI-GF2 to IPs from Hartree−Fock (HF), G_0W_0, and fully self-consistent GW (SCGW) for a set of molecules. In HF theory, the IP is given by the HOMO energy as suggested by Koopmans' theorem. The results for G_0W_0 and SCGW performed over HF are taken from ref 53. The basis set chosen here is cc-pvdz. We have used basis def2-qzvp-ri for fitting the ERI (eq 20) and def2-qzvp-jkfit for fitting the Fock matrix.

We first benchmark our real-time sRI-GF2 results against deterministic GF2 results. In Figure 2, we plot the IP for the

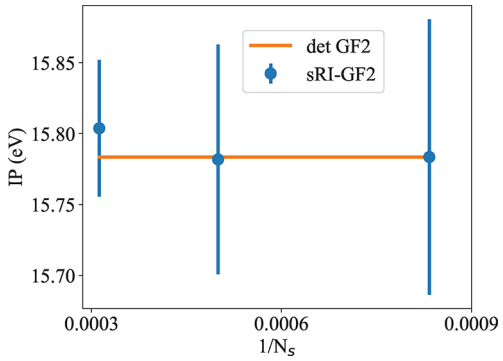

Figure 2. IP for H_2 molecule from sRI-GF2 and deterministic GF2. In sRI-GF2 calculations, we use N_s = 1200, 2000, and 3200 stochastic orbitals. The stochastic error decreases with increasing number of stochastic orbitals.

H_2 molecule from sRI-GF2 results using N_s = 1200, 2000, and 3200 stochastic orbitals. The errors in sRI-GF2 results are estimated by the standard deviation of 10 independent runs using different seeds. As expected, when increasing the number of stochastic orbitals, the errors in sRI-GF2 results decrease. Note that sRI-GF2 predicts IPs in excellent agreement with deterministic GF2 within the error bar.

In Table 1, we list the IPs for a set of selected atoms and molecules. We provide experimental results as well as calculated IPs using HF, G_0W_0, and SCGW and compare these to the real-time sRI-GF2 approach developed herein. The results from sRI-GF2 are mean values of 10 independent runs. The errors from sRI-GF2 are estimated by the standard deviations of the mean values. We also provide the mean absolute error against experimental results. Overall, we find very good agreement between the many-body perturbation techniques based on the GW approximation and the real-time sRI-GF2 approach. The performance of GF2 is comparable and sometimes better than the many-body perturbation technique within the GW approximation. This is a significant observation, since GW is considered the state of the art for describing IPs, even for small molecules.[28,29] This suggests that, for some molecules, a reliable estimate of the IPs can be obtained within a theoretical framework of GF2 without the need to compute screened Coulomb interactions. Note that, in GF2, the dynamic exchange term is included explicitly in self-energy (see Figure 1). To examine the role of dynamic exchange on the IPs, in Table 1 we list IPs for a set of molecules where the dynamic exchange (DE) term in the self-energy was absent. We refer to this as "sRI-GF2 no dynamic exchange (DE)". Note that sRI-GF2 no DE tends to underestimate IPs as compared to sRI-GF2 and experiments. The last column in Table 1 shows the difference in IPs between sRI-GF2 and sRI-GF2 no exchange. These results suggest that the contribution of the dynamic exchange term is significant, up to ≈1 eV corrections to the IPs.

Figure 3 provides a more compelling illustration of the results summarized in Table 1. The horizontal axis in Figure 3 is the experimental IP, and the vertical axis is the IP calculated by the different methods. We find that HF, as expected, overestimates the IP for most molecules studied here. By incorporating electron correlations, the GW and GF2 methods provide much better agreement with experiments.

4.2. Spectral Functions and Computational Complexity: Hydrogen Dimer Chains. While the IP for molecular systems can be obtained using an extended Koopmans' theorem,[37] such a theorem cannot be used to explore the entire frequency range of the spectral function. This brings us to one of the main advantages of the time-domain formalism: With the same computational costs to obtain the IPs, we can also calculate the quasi-particle spectrum over a wide range of frequencies. To demonstrate this within the real-time sRI-GF2, we have carried calculations for the quasi-particle spectrum of a series of hydrogen dimer chains of different lengths, N. We demonstrate that the stochastic RI approach allows us to

Table 1. Ionization Potentials (in eV) for a List of Atoms and Molecules

	expt	HF	G_0W_0	SCGW	sRI-GF2	sRI-GF2 no DE	DE effect
He	24.59	24.88	24.36	24.28	24.01 ± 0.02		
Be	9.32	8.41	8.98	8.46	8.23 ± 0.02		
Ne	21.56	22.64	20.87	20.98	21.44 ± 0.09		
H_2	15.43	16.11	16.23	16.00	15.78 ± 0.03	15.74 ± 0.04	0.04
CH_4	13.60	14.78	14.43	14.09	13.24 ± 0.10	13.16 ± 0.11	0.08
LiH	7.90	8.18	7.96	7.74	7.73 ± 0.02	7.45 ± 0.05	0.28
LiF	11.3	12.66	10.72	10.85	10.77 ± 0.07	9.83 ± 0.10	0.94
HF	16.12	17.11	15.55	15.54	15.19 ± 0.13	15.01 ± 0.19	0.18
H_2O	12.62	13.42	12.17	12.03	11.92 ± 0.10	11.80 ± 0.09	0.12
error	0.00	0.84	0.506	0.51	0.537		

DOI: 10.1021/acs.jctc.9b00918
J. Chem. Theory Comput. 2019, 15, 6703−6711

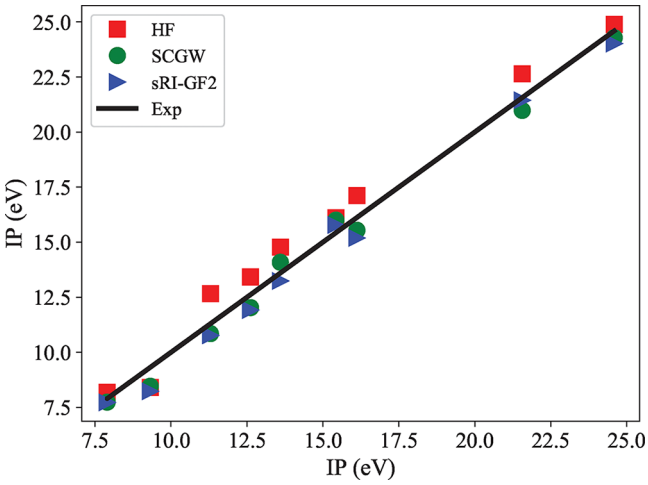

Figure 3. Comparison of IPs calculated from HF, SCGW, and GF2 against experimental results for molecules listed in Table 1. Note that HF tends to overestimate the IP. SCGW and GF2 have similar accuracies in predicting IP.

extend the size of systems that can be described within GF2 with scaling that is slightly better than $O(N_e^3)$.

In ref 41, we have reported on ground state correlation energies for hydrogen dimer chains using stochastic resolution of identity Matsubara second-order Green's function theory. Note that a similar study has been carried out using other methods.[54,55] The same setup will be used in the current work for the real-frequency properties. In short, we set the H−H bond distance to 0.74 Å and the long distance to 2.0 Å. Minimal basis sto-3g is used to represent GFs, and the cc-pvdz-jkfit and cc-pvdz-ri basis sets were used for the Hartree−Fock matrix fitting and for the four-index ERI fitting, respectively. The time step used to propagate the mixed-time GF is $0.2E_h^{-1}$.

In Figure 4, we plot quasi-particle spectrum for a set of hydrogen dimer chains: H_{20}, H_{80}, H_{200}, and H_{300}. For completeness, we also plot the spectrum from HF theory. For small chain lengths we observe individual transitions for both the valence and conduction bands. As the length of the chain increases, these features are washed out (more so for GF2, which contains an imaginary portion to the self-energy which broadens the transitions) and finally a semicontinuous density of states is formed. We also find that the fundamental gap (quasi-particle gap) from GF2 is smaller than that from HF due to electronic correlations.

In Figure 5, we further plot fundamental energy gaps as a function of the length of hydrogen dimer chain from HF and GF2. The fundamental energy gaps are taken as the energy difference between IPs and EAs. We define IP/EA as the frequency position at half the height of peak near HOMO/

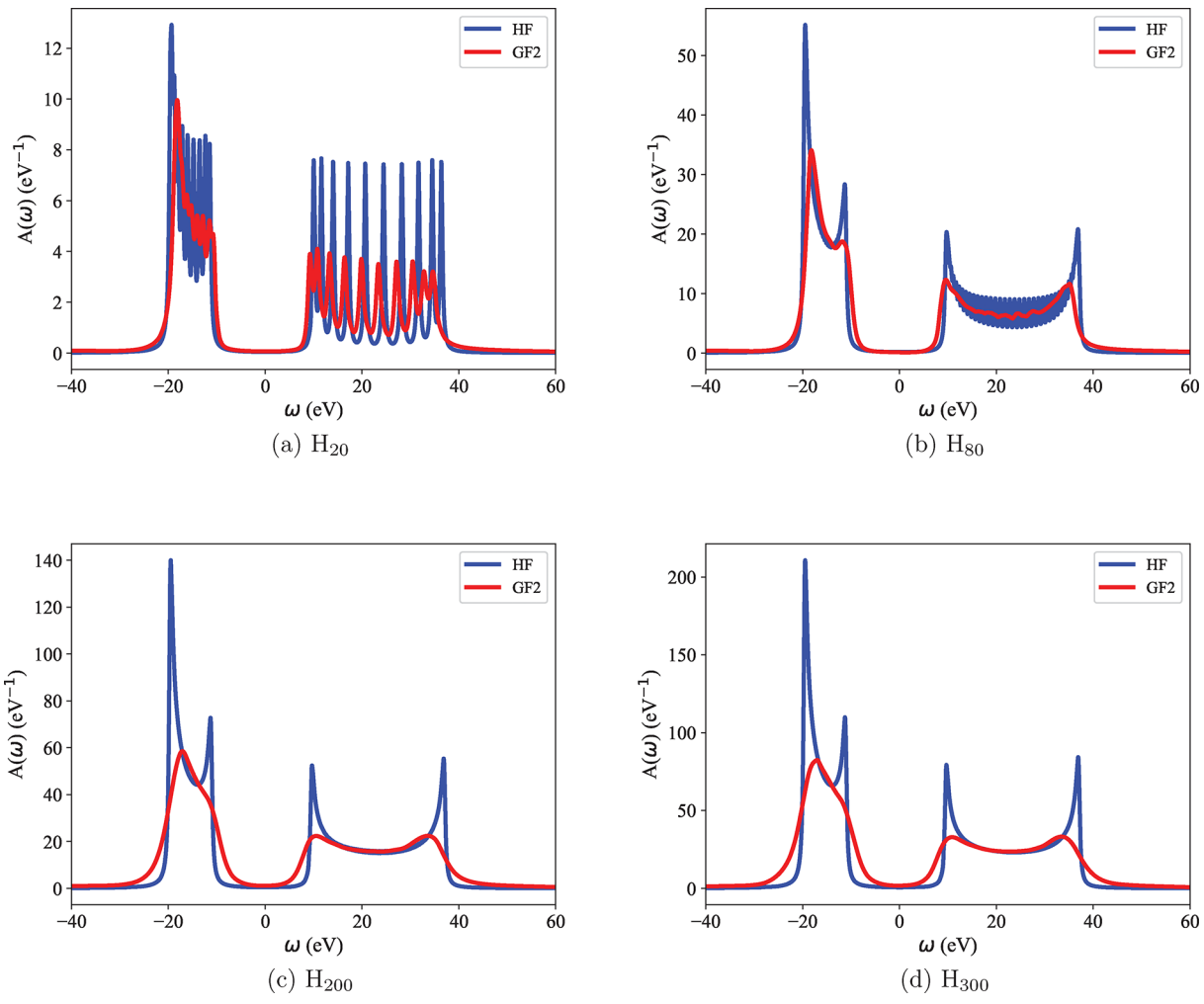

Figure 4. Quasi-particle spectra for H_{20}, H_{80}, H_{200}, and H_{300} using sto-3g basis within the HF (blue curve) and GF2 (red curve) approaches.

DOI: 10.1021/acs.jctc.9b00918
J. Chem. Theory Comput. 2019, 15, 6703−6711

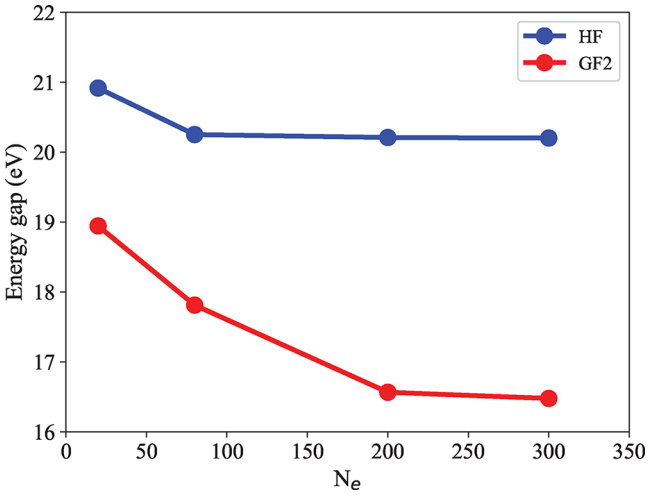

Figure 5. Fundamental energy gaps as a function of number of electrons in the hydrogen dimer chain. Due to incorporation of electron correlations, GF2 predicts smaller fundamental energy gaps as compared to HF. In both cases, energy gaps decrease with the number of hydrogen atoms and converge to a fixed number.

lowest unoccupied molecular orbital (LUMO). As mentioned above, by incorporating electronic correlations, GF2 predicts smaller energy gaps than HF. Note that fundamental energy gaps decrease with the length of the hydrogen dimer chain for both HF and GF2. Note also that fundamental energy gaps from HF converge more quicker than those from GF2 as a function of number of particles.

The computational time and overall scaling of the real-time sRI-GF2 approach are summarized in Figure 6. We plot the

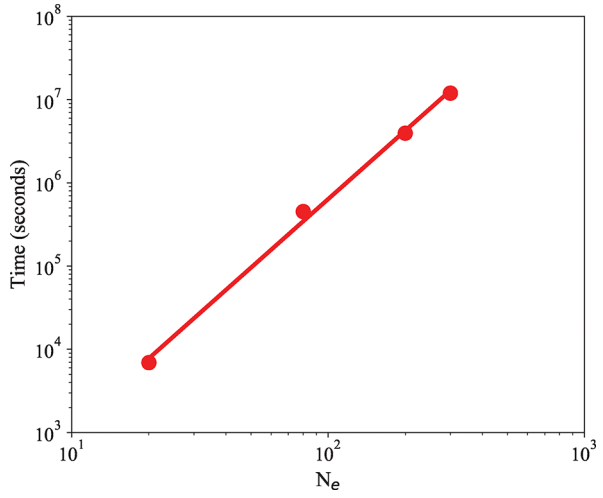

Figure 6. Computational wall time for hydrogen dimer chains. N_e is the number of electrons. The straight line is a power-law fit to the data, suggesting that the scaling is $O(N_e^{2.7})$, slightly better than the theoretical limit of $O(N_e^3)$.

computational wall time as a function of number of hydrogen atoms in the chain, N. These results were generated with 2000 stochastic orbitals to reduce the error to 0.02 eV. We propagate the real-time GFs to $t_{max} = 200E_h^{-1}$, which is sufficient to converge the self-energy to within 10^{-6} eV of it maximal value. As mentioned above, the computational bottleneck for real-time GF propagation is the evaluation of the self-energy in eq 11, which scales as $O(N_e^5)$. The formal scaling using the stochastic RI is $O(N_e^3)$ (see eqs 27 and 28). The results for the hydrogen chain show that in practice the real-time sRI-GF2 scales as $O(N_e^{2.7})$ on multiple 32-core Intel-Xeon CPU E5-2698 v3 at 2.3 GHz nodes.

5. CONCLUSIONS

We have developed a stochastic resolution of identity approach to describe real-time/real-frequency spectral functions of extended systems within the second-order Green's function formalism. The real-time approach provides a platform to compute the ionization potentials and electron affinities for open as well as periodic boundary conditions. Such an approach can also be used to generate the full-frequency quasi-particle spectral function at the same computational cost. The advantage of the stochastic formalism is that it reduces the computational scaling of the real-time sRI-GF2 from $O(N_e^5)$ to $O(N_e^3)$, as illustrated for a chain of hydrogen dimers. This reduced scaling opens the door to study quasi-particle excitations in extended systems within the framework of second-order Green's function.

To access the approach, we benchmarked our real-time sRI-GF2 scheme against a many-body perturbation technique within the GW approximation as well as compared the calculated ionization potentials to experimental results. We find that the sRI-GF2 results are comparable to the state-of-the-art self-consistent GW approach for a set of atoms and small molecules. While GF2 lacks the sort of screening present in the GW approximation, GF2 does include exchange effects in the self-energy, which turn out to be significant in describing the quasi-particle spectrum of molecules.

AUTHOR INFORMATION

Corresponding Authors

*E-mail: douw@berkeley.edu.
*E-mail: tyler.takeshita@daimler.com.
*E-mail: mingchen.chem@berkeley.edu.
*E-mail: roi.baer@huji.ac.il.
*E-mail: dxn@chem.ucla.edu.
*E-mail: eran.rabani@berkeley.edu.

ORCID

Wenjie Dou: 0000-0001-5410-6183
Tyler Y. Takeshita: 0000-0003-0067-2846
Roi Baer: 0000-0001-8432-1925
Eran Rabani: 0000-0003-2031-3525

Funding

R.B. gratefully acknowledges support from the Israel Science Foundation, Grant No. 800/19. D.N. and E.R. are grateful for support by the Center for Computational Study of Excited State Phenomena in Energy Materials (C2SEPEM) at the Lawrence Berkeley National Laboratory, which is funded by the U.S. Department of Energy, Office of Science, Basic Energy Sciences, Materials Sciences and Engineering Division under Contract No. DEAC02-05CH11231 as part of the Computational Materials Sciences Program.

Notes

The authors declare no competing financial interest.

ACKNOWLEDGMENTS

We would like to thank Felipe H. da Jornada and Steven G. Louie for helpful discussion. Resources of the National Energy Research Scientific Computing Center (NERSC), a U.S.

DOI: 10.1021/acs.jctc.9b00918
J. Chem. Theory Comput. 2019, 15, 6703−6711

Department of Energy Office of Science User Facility operated under Contract No. DE-AC02-05CH11231, are greatly acknowledged.

REFERENCES

(1) Dreizler, R. M.; Gross, E. K. *Density Functional Theory: an Approach to the Quantum Many-Body Problem*; Springer Science & Business Media: 2012.

(2) Capelle, K. A bird's-eye view of density-functional theory. *Braz. J. Phys.* **2006**, *36*, 1318−1343.

(3) Koch, W.; Holthausen, M. C. *A Chemist's Guide to Density Functional Theory*; John Wiley & Sons: 2015.

(4) Gidopoulos, N.; Wilson, S. *The Fundamentals of Electron Density, Density Matrix and Density Functional Theory in Atoms, Molecules and the Solid State*; Springer Science & Business Media: 2003; Vol. *14*.

(5) Hohenberg, P.; Kohn, W. Inhomogeneous Electron Gas. *Phys. Rev.* **1964**, *136*, B864−B871.

(6) Kohn, W.; Sham, L. J. Self-consistent equations including exchange and correlation effects. *Phys. Rev.* **1965**, *140*, A1133.

(7) Perdew, J. P.; Parr, R. G.; Levy, M.; Balduz, J. L. Density-Functional Theory for Fractional Particle Number: Derivative Discontinuities of the Energy. *Phys. Rev. Lett.* **1982**, *49*, 1691−1694.

(8) Cohen, A. J.; Mori-Sánchez, P.; Yang, W. Fractional charge perspective on the band gap in density-functional theory. *Phys. Rev. B: Condens. Matter Mater. Phys.* **2008**, *77*, 115123.

(9) Seidl, A.; Görling, A.; Vogl, P.; Majewski, J.; Levy, M. Generalized Kohn-Sham schemes and the band-gap problem. *Phys. Rev. B: Condens. Matter Mater. Phys.* **1996**, *53*, 3764.

(10) Hedin, L. New Method for Calculating the One-Particle Green's Function with Application to the Electron-Gas Problem. *Phys. Rev.* **1965**, *139*, A796−A823.

(11) Hybertsen, M. S.; Louie, S. G. First-principles theory of quasiparticles: calculation of band gaps in semiconductors and insulators. *Phys. Rev. Lett.* **1985**, *55*, 1418.

(12) Hybertsen, M. S.; Louie, S. G. Electron correlation in semiconductors and insulators: Band gaps and quasiparticle energies. *Phys. Rev. B: Condens. Matter Mater. Phys.* **1986**, *34*, 5390.

(13) Rieger, M. M.; Steinbeck, L.; White, I.; Rojas, H.; Godby, R. The GW space-time method for the self-energy of large systems. *Comput. Phys. Commun.* **1999**, *117*, 211−228.

(14) Rinke, P.; Qteish, A.; Neugebauer, J.; Freysoldt, C.; Scheffler, M. Combining GW calculations with exact-exchange density-functional theory: an analysis of valence-band photoemission for compound semiconductors. *New J. Phys.* **2005**, *7*, 126.

(15) Neaton, J. B.; Hybertsen, M. S.; Louie, S. G. Renormalization of molecular electronic levels at metal-molecule interfaces. *Phys. Rev. Lett.* **2006**, *97*, 216405.

(16) Tiago, M. L.; Chelikowsky, J. R. Optical excitations in organic molecules, clusters, and defects studied by first-principles Green's function methods. *Phys. Rev. B: Condens. Matter Mater. Phys.* **2006**, *73*, 205334.

(17) Friedrich, C.; Schindlmayr, A.; Blügel, S.; Kotani, T. Elimination of the linearization error in GW calculations based on the linearized augmented-plane-wave method. *Phys. Rev. B: Condens. Matter Mater. Phys.* **2006**, *74*, 045104.

(18) Grüning, M.; Marini, A.; Rubio, A. Density functionals from many-body perturbation theory: The band gap for semiconductors and insulators. *J. Chem. Phys.* **2006**, *124*, 154108.

(19) Shishkin, M.; Kresse, G. Self-consistent G W calculations for semiconductors and insulators. *Phys. Rev. B: Condens. Matter Mater. Phys.* **2007**, *75*, 235102.

(20) Rostgaard, C.; Jacobsen, K. W.; Thygesen, K. S. Fully self-consistent GW calculations for molecules. *Phys. Rev. B: Condens. Matter Mater. Phys.* **2010**, *81*, 085103.

(21) Tamblyn, I.; Darancet, P.; Quek, S. Y.; Bonev, S. A.; Neaton, J. B. Electronic energy level alignment at metal-molecule interfaces with a G W approach. *Phys. Rev. B: Condens. Matter Mater. Phys.* **2011**, *84*, 201402.

(22) Liao, P.; Carter, E. A. Testing variations of the GW approximation on strongly correlated transition metal oxides: hematite (α-Fe 2 O 3) as a benchmark. *Phys. Chem. Chem. Phys.* **2011**, *13*, 15189−15199.

(23) Refaely-Abramson, S.; Baer, R.; Kronik, L. Fundamental and excitation gaps in molecules of relevance for organic photovoltaics from an optimally tuned range-separated hybrid functional. *Phys. Rev. B: Condens. Matter Mater. Phys.* **2011**, *84*, 075144.

(24) Marom, N.; Caruso, F.; Ren, X.; Hofmann, O. T.; Körzdörfer, T.; Chelikowsky, J. R.; Rubio, A.; Scheffler, M.; Rinke, P. Benchmark of G W methods for azabenzenes. *Phys. Rev. B: Condens. Matter Mater. Phys.* **2012**, *86*, 245127.

(25) Isseroff, L. Y.; Carter, E. A. Importance of reference Hamiltonians containing exact exchange for accurate one-shot G W calculations of Cu 2 O. *Phys. Rev. B: Condens. Matter Mater. Phys.* **2012**, *85*, 235142.

(26) Refaely-Abramson, S.; Sharifzadeh, S.; Govind, N.; Autschbach, J.; Neaton, J. B.; Baer, R.; Kronik, L. Quasiparticle spectra from a nonempirical optimally tuned range-separated hybrid density functional. *Phys. Rev. Lett.* **2012**, *109*, 226405.

(27) Kronik, L.; Stein, T.; Refaely-Abramson, S.; Baer, R. Excitation gaps of finite-sized systems from optimally tuned range-separated hybrid functionals. *J. Chem. Theory Comput.* **2012**, *8*, 1515−1531.

(28) van Setten, M. J.; Caruso, F.; Sharifzadeh, S.; Ren, X.; Scheffler, M.; Liu, F.; Lischner, J.; Lin, L.; Deslippe, J. R.; Louie, S. G.; Yang, C.; Weigend, F.; Neaton, J. B.; Evers, F.; Rinke, P. GW 100: Benchmarking G 0 W 0 for molecular systems. *J. Chem. Theory Comput.* **2015**, *11*, 5665−5687.

(29) Vlcek, V.; Rabani, E.; Neuhauser, D.; Baer, R. Stochastic GW calculations for molecules. *J. Chem. Theory Comput.* **2017**, *13*, 4997−5003.

(30) Cederbaum, L. One-body Green's function for atoms and molecules: theory and application. *J. Phys. B: At. Mol. Phys.* **1975**, *8*, 290.

(31) Holleboom, L.; Snijders, J. A comparison between the Møller−Plesset and Green's function perturbative approaches to the calculation of the correlation energy in the many-electron problem. *J. Chem. Phys.* **1990**, *93*, 5826−5837.

(32) Stefanucci, G.; van Leeuwen, R. *Nonequilibrium Many-Body Theory of Quantum Systems: A Modern Introduction*; Cambridge University Press: 2013.

(33) Dahlen, N. E.; van Leeuwen, R.; von Barth, U. Variational energy functionals of the Green function tested on molecules. *Int. J. Quantum Chem.* **2005**, *101*, 512−519.

(34) Phillips, J. J.; Zgid, D. Communication: The description of strong correlation within self-consistent Green's function second-order perturbation theory. *J. Chem. Phys.* **2014**, *140*, 241101.

(35) Pavošević, F.; Peng, C.; Ortiz, J.; Valeev, E. F. Communication: Explicitly correlated formalism for second-order single-particle Green's function. *J. Chem. Phys.* **2017**, *147*, 121101.

(36) Ohnishi, Y.-y.; Ten-no, S. Explicitly correlated frequency-independent second-order green's function for accurate ionization energies. *J. Comput. Chem.* **2016**, *37*, 2447−2453.

(37) Welden, A. R.; Phillips, J. J.; Zgid, D. Ionization potentials and electron affinities from the extended Koopmans' theorem in self-consistent Green's function theory. 2015, arXiv:1505.05575. arXiv.org e-Print archive. https://arxiv.org/abs/1505.05575.

(38) Dahlen, N. E.; van Leeuwen, R. Self-consistent solution of the Dyson equation for atoms and molecules within a conserving approximation. *J. Chem. Phys.* **2005**, *122*, 164102.

(39) Neuhauser, D.; Baer, R.; Zgid, D. Stochastic self-consistent second-order Green's function method for correlation energies of large electronic systems. *J. Chem. Theory Comput.* **2017**, *13*, 5396−5403.

(40) Takeshita, T. Y.; de Jong, W. A.; Neuhauser, D.; Baer, R.; Rabani, E. Stochastic formulation of the resolution of identity: Application to second order Møller−Plesset perturbation theory. *J. Chem. Theory Comput.* **2017**, *13*, 4605−4610.

DOI: 10.1021/acs.jctc.9b00918
J. Chem. Theory Comput. 2019, 15, 6703−6711

(41) Takeshita, T. Y.; Dou, W.; Smith, D. G.; de Jong, W. A.; Baer, R.; Neuhauser, D.; Rabani, E. Stochastic resolution of identity second-order Matsubara Green's function theory. *J. Chem. Phys.* **2019**, *151*, 044114.
(42) Neuhauser, D.; Rabani, E.; Baer, R. Expeditious stochastic approach for MP2 energies in large electronic systems. *J. Chem. Theory Comput.* **2013**, *9*, 24−27.
(43) Ge, Q.; Gao, Y.; Baer, R.; Rabani, E.; Neuhauser, D. A guided stochastic energy-domain formulation of the second order Møller−Plesset perturbation theory. *J. Phys. Chem. Lett.* **2014**, *5*, 185−189.
(44) Neuhauser, D.; Rabani, E.; Baer, R. Expeditious Stochastic Calculation of Random-Phase Approximation Energies for Thousands of Electrons in Three Dimensions. *J. Phys. Chem. Lett.* **2013**, *4*, 1172−1176.
(45) Baer, R.; Neuhauser, D.; Rabani, E. Self-Averaging Stochastic Kohn-Sham Density-Functional Theory. *Phys. Rev. Lett.* **2013**, *111*, 106402.
(46) Neuhauser, D.; Baer, R.; Rabani, E. Embedded fragment stochastic density functional theory. *J. Chem. Phys.* **2014**, *141*, 041102.
(47) Cytter, Y.; Neuhauser, D.; Baer, R. Metropolis evaluation of the hartree−fock exchange energy. *J. Chem. Theory Comput.* **2014**, *10*, 4317−4323.
(48) Chen, M.; Baer, R.; Neuhauser, D.; Rabani, E. Overlapped embedded fragment stochastic density functional theory for covalently-bonded materials. *J. Chem. Phys.* **2019**, *150*, 034106.
(49) Neuhauser, D.; Gao, Y.; Arntsen, C.; Karshenas, C.; Rabani, E.; Baer, R. Breaking the Theoretical Scaling Limit for Predicting Quasiparticle Energies: The Stochastic *GW* Approach. *Phys. Rev. Lett.* **2014**, *113*, 076402.
(50) Haug, H.; Jauho, A.-P. *Quantum Kinetics in Transport and Optics of Semiconductors*; Springer: 2008; Vol. 2.
(51) Stan, A.; Dahlen, N. E.; Van Leeuwen, R. Time propagation of the Kadanoff−Baym equations for inhomogeneous systems. *J. Chem. Phys.* **2009**, *130*, 224101.
(52) We have set $t_{ce} = 100E_h^{-1}$ in our calculations.
(53) Koval, P.; Foerster, D.; Sánchez-Portal, D. Fully self-consistent *GW* and quasiparticle self-consistent *GW* for molecules. *Phys. Rev. B: Condens. Matter Mater. Phys.* **2014**, *89*, 155417.
(54) LeBlanc, J. P. F.; et al. Solutions of the Two-Dimensional Hubbard Model: Benchmarks and Results from a Wide Range of Numerical Algorithms. *Phys. Rev. X* **2015**, *5*, 041041.
(55) Motta, M.; et al. Towards the Solution of the Many-Electron Problem in Real Materials: Equation of State of the Hydrogen Chain with State-of-the-Art Many-Body Methods. *Phys. Rev. X* **2017**, *7*, 031059.

DOI: 10.1021/acs.jctc.9b00918
J. Chem. Theory Comput. 2019, 15, 6703−6711